coatings

MDPI

Article

Effect of Particle Size on the Thermal Shock Resistance of Plasma-Sprayed YSZ Coatings

Jibo Huang [1], Weize Wang [1,*], Xiang Lu [1], Doudou Hu [1], Zhengqu Feng [1] and Tianxu Guo [2]

[1] Key Laboratory of Pressure System and Safety, Ministry of Education, East China University of Science and Technology, Shanghai 200237, China; Y20150084@mail.ecust.edu.cn (J.H.); Y45160090@mail.ecust.edu.cn (X.L.); 10131805@mail.ecust.edu.cn (D.H.); fengzhengqu@shanghai-fanuc.com.cn (Z.F.)

[2] Shanghai Junshan Surface Technology Engineering Co., Ltd., Shanghai 201900, China; Jsb02@shjsst.com

* Correspondence: wangwz@ecust.edu.cn; Tel.: +86-21-6425-2819

Received: 18 August 2017; Accepted: 18 September 2017; Published: 19 September 2017

Abstract: In this study, yttria-stabilized zirconia (YSZ) coatings were deposited by atmospheric plasma spraying (APS) using feedstocks with two different particle sizes. The effect of particle size on the pore structure and failure mechanism of the coatings was investigated. The evolution of the pore structure of the two kinds of coatings during cyclic thermal shock test was described by quantitative metallography. The influence of pore orientation on the thermal stress of the coating system was analyzed by the finite element method. It was found that the coatings deposited using coarse particles show a high thermal shock life time. The orientation of the pores in the coatings prepared by different particle sizes was different. A structural parameter was proposed to effectively characterize the pore orientation of the coatings. Coatings prepared by coarse YSZ powder tend to form almost the same number of horizontal and vertical pores, while coatings prepared by fine powder tend to form horizontal ones parallel to the direction of the substrate. The simulation results revealed that the vertical pores can reduce the thermal stress in the coating. The results of this investigation are a benefit to the design and integrity of TBCs.

Keywords: thermal barrier coatings; YSZ; particle size; pore; thermal shocks; stress

1. Introduction

The thermal barrier coatings (TBCs) are widely used in hot sections of gas-turbine engines to improve their operating temperature and provide thermal protection for the underlying metallic components, thereby improving the efficiency and performance of the engine [1,2]. The TBC systems generally consist of four layers which are the substrate, the bond coat (BC), the thermally-grown oxide (TGO), and the ceramic top coat (TC) [1]. Due to the thermal expansion coefficient difference between the ceramic coating and the metallic material, thermal mismatch stress appears in the coating system under cyclic thermal shock conditions, resulting in the cracking and peeling of the ceramic layer [3,4]. Plasma-sprayed TBCs are widely used due to their low production cost and versatility. In this method, YSZ powders are carried by an inert gas mixture into the plasma plume where they are melted, accelerated, and propelled against a substrate. The molten particles impact and solidify on the substrate creating the characteristic lamellar microstructure with a typical porosity of 10%–20% [5,6]. The pores in a plasma-sprayed coating can be divided into three types with various orientations and shapes: intra-lamellar cracks, inter-lamellar pores and globular pores [7–9]. In addition, the pore structure of the coating may evolve during the thermal cycling due to the effect of sintering and thermal stress [10,11]. The increase in stiffness caused by the sintering of fine-scale porosity has significant impact on the strain tolerance of the TBC [12].

Generally, the existence of pores degrades the mechanical properties of materials and alters the failure mechanisms of TBCs [13–15]. Due to the presence of a large number of pores parallel to the substrate, APS TBCs usually has a shorter thermal shock life than the electron beam-physical-vapor-deposited (EB-PVD) coating [1,16]. However, the thermal shock resistance of plasma sprayed TBCs can be improved by optimizing the pore structure in the ceramic layer [17,18]. In addition, the pores in the ceramic layer can reduce its thermal conductivity and improve the strain tolerance of the coating [19,20], which can be fulfilled by adjusting the spraying parameters, adopting specific YSZ powder and coating post-processing [21–24]. The strain tolerance of coatings can also be improved through introducing vertical cracks in the ceramic coating by means of surface heating [25,26]. However, the segmented coatings are denser than traditionally plasma-sprayed TBCs due to its good in-splat bonding at high substrate temperature. In addition, some branching cracks parallel to the substrate are inevitably formed in the coating [27]. Lisa Pin el al. deposited the YSZ layer via sol-gel method, cracked the coating by high temperature sintering, and filled up those cracks by plasma sprayed YSZ coating to reinforce the original micro-crack network, giving rise to the similar thermal cycle life with EB-PVD TBCs [28,29]. These publications show that the thermal shock resistance can be improved by tailoring the microstructure of the TBC system.

At present, the main parameters describing the pore structure of the coating are porosity, bonding ratio, and micro-crack density [30–33], etc. These parameters can effectively describe the specific pore structure in the coating. It should be noted that pore orientation is also an important feature that affects the thermal shock resistance of TBCs. However, until now, parameters that can effectively describe this feature are quite limited.

The particle size affects the deposition, solidification, and crystallization of molten droplets by influencing the size of deposited particles, thus affecting the microstructure of the coatings [34]. Fine particles typically result in good melting during deposition, and further the low porosity for coatings due to the decreased volume of inter-splats gaps and voids [25]. Correspondingly, the coatings deposited from fine powder exhibit higher fracture toughness compared to the coating deposited from coarse powder [35]. In general, high fracture toughness can retard the crack propagation, but the lifetime and failure behavior of TBCs are dominated by the competition between driving force and cracking resistance [36]. Many studies have shown that the thermal shock resistance of TBCs with dense ceramic top coat is worse than that with porous top coat [13,15,21]. Our previous study has revealed the effect of particle size on cracking of TBCs during cyclic thermal shock test [15]. Due to the variation of pore structure, an incubation period exists in the coatings made from the coarse powder, which postpone the onset of rapid cracking of the coating [15]. In order to further understand the effect of pore structure on the failure of TBCs, in this study, YSZ coatings with different microstructure were deposited via different sizes of particles, and the evolution of pore structure during cyclic thermal shock testing was investigated. In addition, the effect of pore orientation on the stress state of the coating was analyzed by means of the finite element method (FEM).

2. Materials and Methods

2.1. Preparation of Coatings

A 3 mm thick and 25.4 mm diameter disc of IN-738 nickel-based super alloy was employed as the substrate. For the TBCs, a commercial agglomeration sintered ZrO_2 8 wt % Y_2O_3 (8YSZ) powder (Chengdu HuaYin Powder Technology Co., Ltd., Chengdu, China) was used to deposit the ceramic top coat. Prior to the deposition of the top-coat, a commercially-available NiCrAlY powder (45–106 μm, Beijing SunSpraying New Material Co., Ltd., Beijing, China) was used as the bond coat. To study the effect of particle size on the coating microstructure, YSZ powders with different particle size ranges were selected using the sieving method. The powder with particle size ranges of 15–25 μm and 45–60 μm (shown as Figure 1) are named as the fine and coarse powder, respectively. Both the YSZ top coat and the bond coat were deposited by a commercial air plasma spray (APS) system (APS-2000,

Beijing Aeronautical Manufacturing Technology Research Institute, Beijing, China) onto the substrate. During spraying, argon was used as the main gas and hydrogen as the auxiliary gas. The pressure was controlled at 0.4 MPa and 0.25 MPa, respectively. The main gas flow was controlled at 47 L/min. Argon was also used as the powder feed gas with a flow rate of 9 L/min. The plasma power was maintained at approximately 36 kW (600 A/60 V) and 30 kW (500 A/60 V) to deposit the YSZ and the bond coat, respectively. The traverse speed of the spray gun was kept as 150 mm/s with a spray distance of 100 mm for the bond coat deposition and 70 mm for YSZ deposition. For all of the samples, the thickness of the bond coat and the top coat was approximately 150 μm and 300 μm, respectively. A heat pre-treatment of TBC samples was carried out at a temperature of 1050 °C for 4 h in a vacuum atmosphere to control the uniform formation of α-alumina-based TGO at the interface between the bond coat and YSZ and to release the residual stress in the coating.

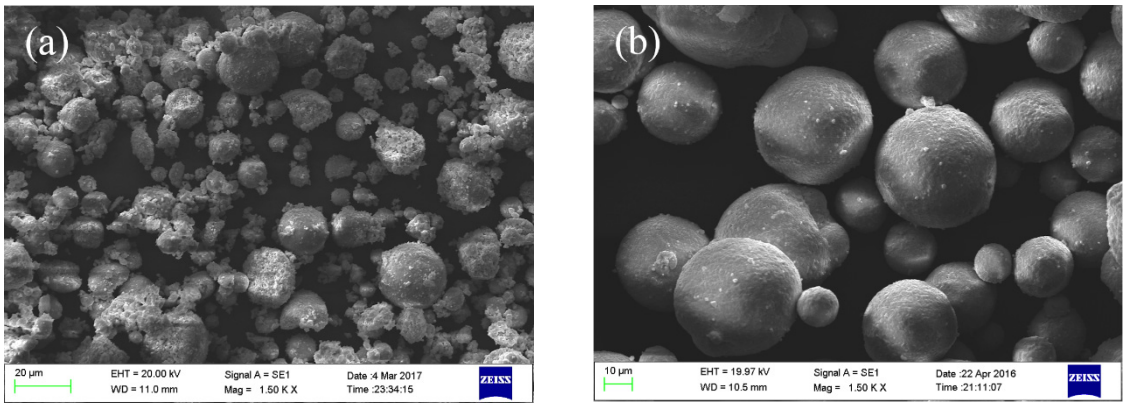

Figure 1. Morphologies of the 8YSZ powders. (**a**) Particle size ranging 15–25 μm; (**b**) Particle size ranging 45–60 μm.

2.2. Cyclic Thermal Shock Test

Thermal shock resistance of coatings was evaluated by cyclic thermal shock testing. Thermal shock tests were conducted using a muffle furnace. When the temperature of the furnace reached 1080 °C, the samples were put into the furnace. The dwell time at high temperature was 30 min. After heating, the samples were directly quenched into deionized water. The failure criteria for the coatings are defined as cracking and peeling off by visual inspection. The thermal shock life of each coating was determined using three samples.

2.3. Pore Structure Analysis

In order to determine the evolution of the pore structure in coatings, TBC samples were taken out periodically and sectioned by a low-speed, high-precision diamond saw. Then the mounted sample was ground and polished using the standard metallography procedure. Before cutting samples, the coating was cured with E7 glue to avoid the introduction of new cracks and pores during the cutting and metallographic preparation processes. The cross-sectional structure of coatings was observed using a scanning electron microscope (SEM, ZEISS EVO MA15, Carl Zeiss SMT Ltd., Cambridge, UK) in the backscattered and secondary electron modes with an acceleration voltage of 20 kV. Image analysis is demonstrated to be a convenient and reliable means for microstructural characterization of thermal spray coatings [37]. Pore size, shape, orientation, and distribution can be assessed through using image analysis from typical images taken at sufficiently high magnification. In this study, the pore structure of coatings prepared by two kinds of YSZ powder all showed complex dendrimer morphology, and the orientation of the pores in the coatings prepared by different particle sizes was obviously different. The feature of pores orientation in the coating were quantitatively analyzed by image analysis.

Image Pro Plus 6.0 software was used to quantitatively measure the pore structure of SEM images with a magnification of 1000 times. The image processing includes image segmentation and filtering. Image segmentation was performed by thresholding leading to binary images. In order to minimize the effects of the possibly generated artefacts, the threshold to extract the pores from the background was manually sifted from a grey level of 0–1, by carefully comparing the produced binary image with the original grey level image [38]. Taking the heat-treated coating prepared by coarse particle size as an example, the extracting pore structure (black area) from the original SEM image of Figure 2a is shown in Figure 2b. Then the orientation information of the pores was obtained through the Image-Pro Plus 6.0 software by measuring the angle between the principal axis of the pore and the horizontal direction which is perpendicular to the spray gun, as show in Figure 3a, and then classify the pore directly through the angle. The pore with the angle between 0° and 45° are considered to be a horizontal pore. Otherwise, it belongs to the vertical one. As show in Figure 3b,c, pores have been divided into horizontal and vertical pores (the red area in the image) on the basis of this method. Through the measurement of the software, the content of the pores within any angle range can be obtained.

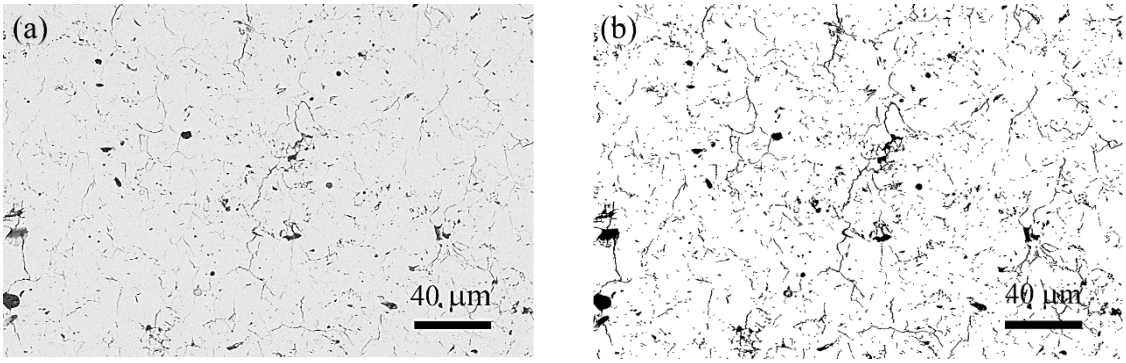

Figure 2. The process of extracting the pore characteristics of the coating (45–60 μm, after heat pre-treatment): (**a**) SEM image and (**b**) image binarization and extraction of pores.

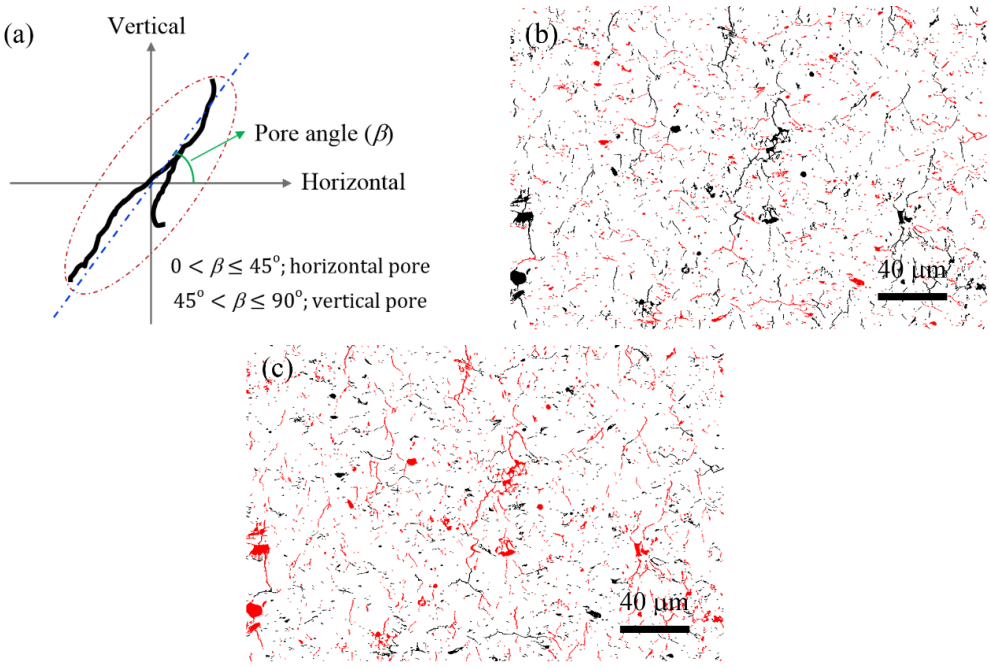

Figure 3. Schematic diagrams of methods to classify pores by (**a**) orientation feature: the effect of dividing pores into (**b**) horizontal and (**c**) vertical pores.

2.4. Finite Element Analysis

Thermal barrier coatings are subjected to thermal stresses during thermal shocks due to the different material properties and uneven temperature distribution of each layer. The influence of the orientation of the pores in the ceramic coating on the thermal stress of the TBC system was analyzed by the finite element method. The model employed in the finite element analysis is shown in Figure 4. In the simulation process, the thermal stress of TBC system with different pore orientation was calculated. The angles between the pores and the substrate direction are set as 0°, 30°, 45°, 60°, and 90°, respectively. The structure of the pores in the ceramic layer is shown as Figure 4. All the pores are simplified to a rectangular with a length and a width of 30 and 0.5 μm according to the crack observation. The location of the pores in the coating is the same in order to compare the effect of pore orientation.

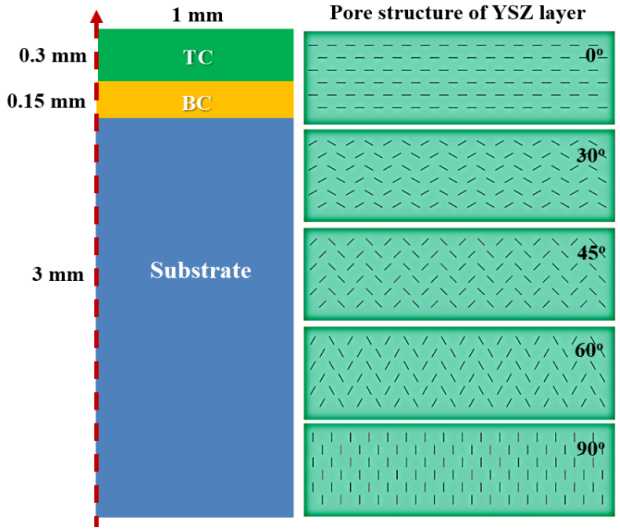

Figure 4. Schematic illustration of a TBC specimen and its pore structure in TC layer.

During the FEM analysis in ABAQUS 6.10, temperature distribution was achieved firstly by transient heat transfer analysis, and then the stress distribution was obtained by using the temperature field as an input load. During thermal cycling, the heat exchange between the sample and its surrounding environment was carried out by convection, and that between layers of the coating was by conduction. Heat exchange by radiative is neglected in this study. The heating stage was used to simulate the heating of the sample into a muffle furnace at a temperature of 1080 °C. The convective heat transfer coefficient between the sample surface and the hot air was taken as 110 W/m^2 °C, according to [4]. While in cooling stage, the heat transfer coefficient was assumed to be 1000 W/m^2 °C to simulate putting a sample into water at a temperature of 20 °C from the furnace. During the stress analysis, the left boundary of the model was set as a symmetric boundary, and other boundaries were all set as free boundaries. Considering that the model was pore-contained structure, the Young's modulus and thermal conductivity of YSZ coating were chosen as E_o = 200 GPa, K_o = 2.3 W/mK, respectively, according to the bulk YSZ material [39]. Other material properties used in the simulation process were all referred to the parameters given in [40].

3. Results and Discussion

3.1. Microstructure Analysis

Figure 5a,b shows the microstructure of as-sprayed 8YSZ coatings deposited from powders with different sizes. Most of the pores in the as-sprayed coatings are formed due to incomplete stacking

of splats and the gas trapped in melt particles during deposition. More large spherical and irregular voids can be found in the coatings deposited from the coarse powder than that deposited from the fine powder. The number of pores in the coatings prepared by fine YSZ is greater, while the volume of them seems to be smaller.

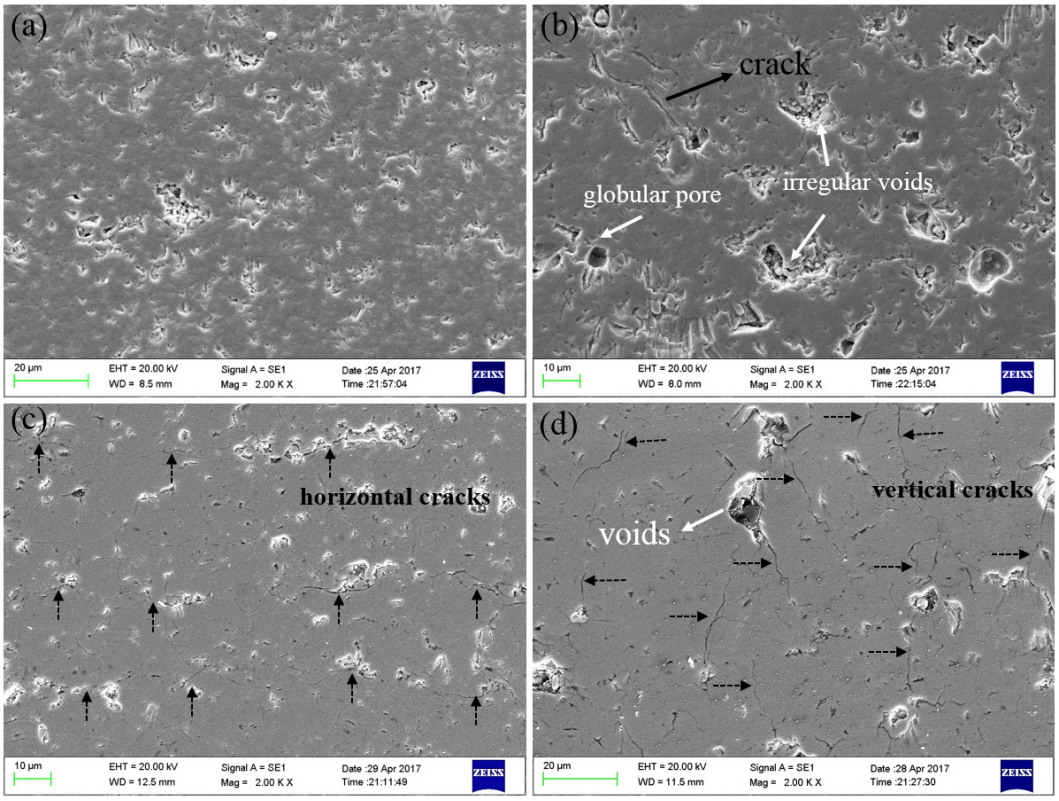

Figure 5. Typical microstructures of the YSZ coating: (**a**) As-sprayed, 15–25 μm; (**b**) as-sprayed, 45–60 μm; (**c**) after heat pre-treatment, 15–25 μm; and (**d**) after heat pre-treatment, 45–60 μm.

The microstructure of the coatings after heat treatment is shown in Figure 5c,d. Compared to the as-sprayed coating, the coating after heat treatment becomes denser due to the sintering effect during the high-temperature operation. The sintering results in the disappearance of fine pores, while the large ones still remain in the coating. It is interesting to notice that some micro-cracks were formed in the coatings, which is probably due to the sintering shrinkage and thermal stress. However, the orientation distributions of these crack-like pores formed in the coatings prepared by the two particle sizes are obviously different. Coatings prepared by coarse YSZ powder tend to form intra-splat cracks with direction perpendicular to the substrate, while coatings prepared by fine powder tend to form inter-splat cracks parallel to the substrate.

The fracture morphology of the coatings after failure is shown in Figure 6. It can also be observed that the coatings prepared by fine YSZ powder are denser than those prepared by coarse powder. Some large inter-lamellar cracks were generated in the coatings prepared by fine YSZ powder due to the propagation of inter-splat micro-cracks. In contrast, the micro-cracks in the coatings prepared by coarse powder did not propagate and coalesce obviously, and almost no coating damage could be found.

The difference in the pore orientation of the coatings deposited from the two particle size powders may relate with the difference in the stacking morphology of the splats. As can be seen from Figure 7, the surface of the coating prepared by the coarse YSZ powder (Figure 7a) is rougher than that prepared by the fine powder (Figure 7b), which can infer that the interfaces between the lamellar prepared by coarse particle size are more tortuous. The rough interface may facilitate increasing the mechanical

bonding strength between the following deposited splats and the previously formed coating. Therefore, during the thermal shocks, cracks in the coating prepared by the coarse powder are difficult to expand along the lamellar interface (parallel to the substrate). Instead, some intra-splat cracks perpendicular to the substrate are formed. However, in the coatings prepared by the fine powder, due to the smooth lamellar interface, the crack propagation resistance along the interface is weak, so it tends to form inter-lamellar cracks in the direction of the parallel to the substrate.

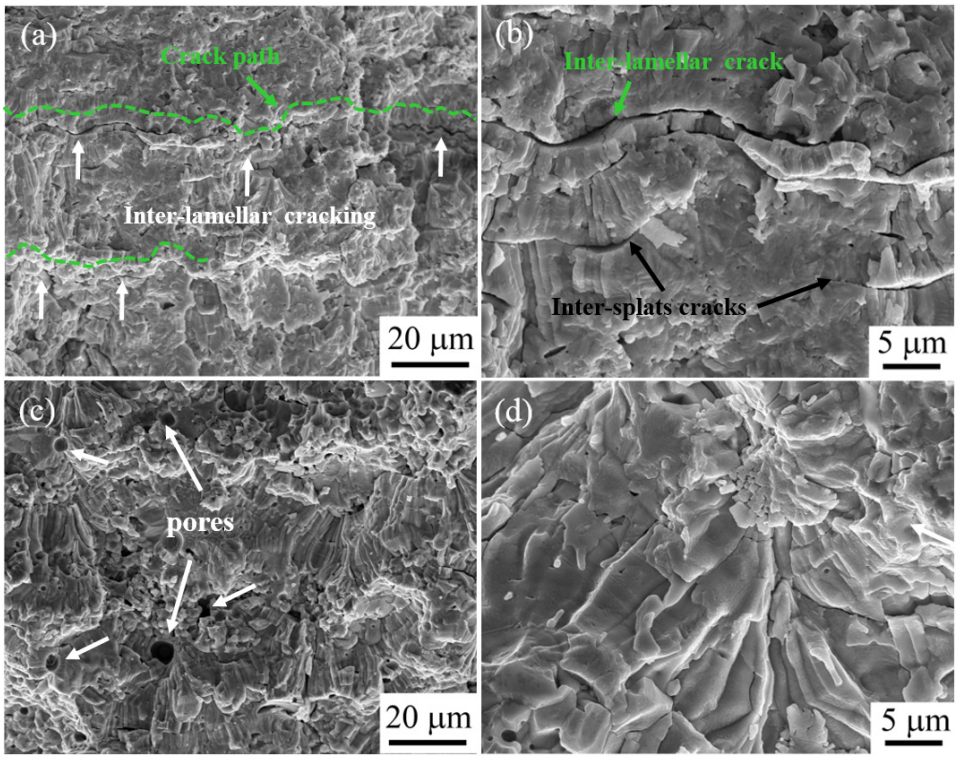

Figure 6. Typical fracture morphologies of the coating after failure at different magnifications: (**a**,**b**) 15–25 μm; and (**c**,**d**) 45–60 μm.

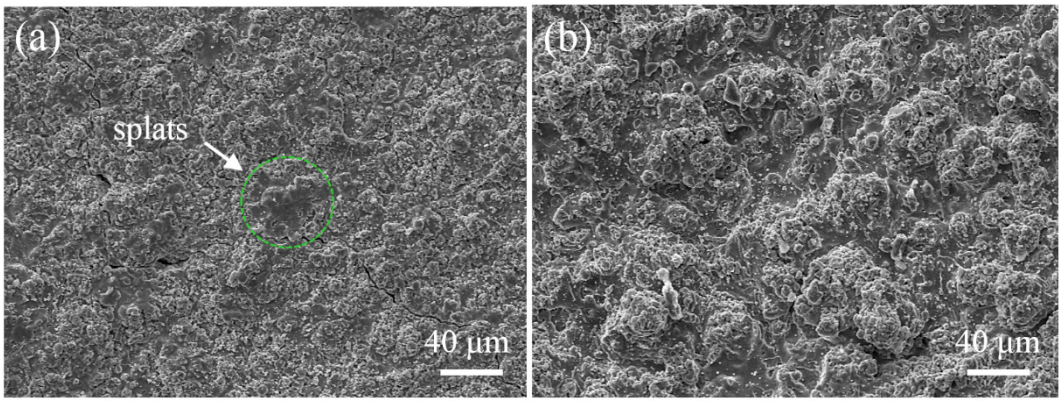

Figure 7. Typical surface morphologies of the coating after failure: (**a**) 15–25 μm; and (**b**) 45–60 μm.

3.2. Porosity

Through cyclic thermal shock test, it was found that all three samples of the coating prepared with fine YSZ powder were cracked after 27 cycles of thermal shock, while the lifetime of three samples deposited from coarse powder were 37, 37, and 39 times, respectively. The pore structure of the coating

affects the thermal shock life of the thermal barrier coating. Figure 8 shows the pore structure of YSZ coatings deposited from the two different size of powder at specific thermal cycles. The pores in the coating after thermal shock contain the initial ones formed during the deposition process and the micro-cracks generated during cyclic thermal shock test. By means of the pore structure analysis method in Section 2.3, the evolution of total porosity and corresponding percentages of horizontal and vertical pores in coatings prepared by different YSZ powder are obtained (shown in Figure 9). It can be seen that the porosity of the two kinds of YSZ coatings declines after heat treatment and then increases with the number of thermal shock cycles increasing. The decrease of porosity after heat treatment is due to sintering at high temperature, and the increase of porosity resulted from the formation of micro-cracks under thermal stress during thermal shock. Due to the large number of inter-lamellar cracks in the coating prepared by the fine YSZ powder, the total porosity of the coating after thermal shock is slightly higher than that deposited from coarse YSZ.

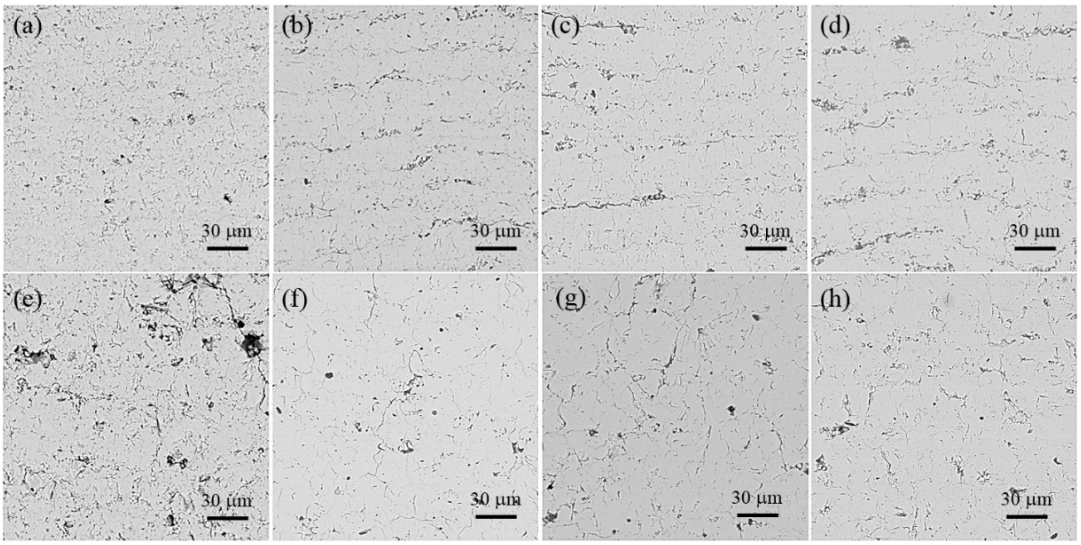

Figure 8. Pore structure of YSZ coatings deposited from two different size of powder after different thermal shock cycles: (**a**) As-sprayed, 15–25 μm; (**b**) after heat pre-treatment, 15–25 μm; (**c**) 20 cycles, 15–25 μm; (**d**) 27 cycles, 15–25 μm; (**e**) as-sprayed, 45–60 μm; (**f**) after heat pre-treatment, 45–60 μm; (**g**) 20 cycles, 45–60 μm; and (**h**) 39 cycles, 45–60 μm.

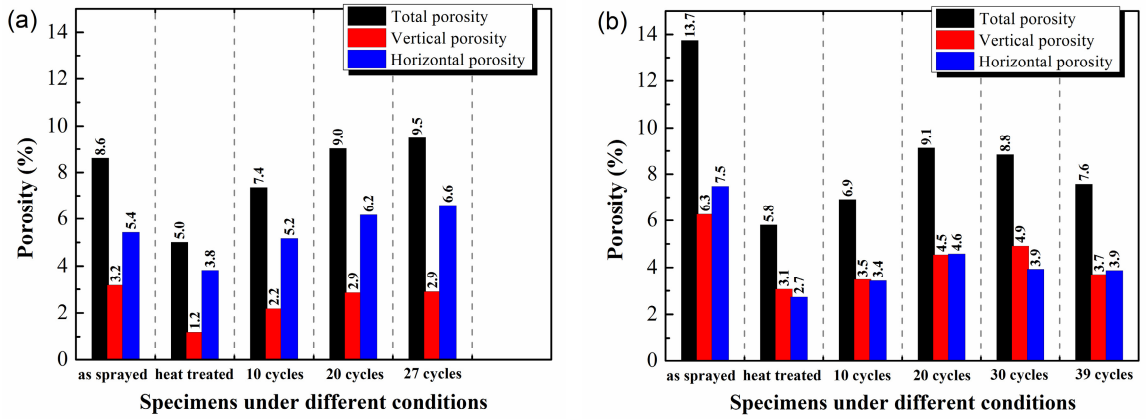

Figure 9. Evolution of pore structure of the two kinds of coatings during thermal shock test: (**a**) 15–25 μm and (**b**) 45–60 μm.

After the heat pre-treatment, the proportion of horizontal pores is about two-thirds of the total porosity in the coatings prepared by fine YSZ powder. In contrast, the coatings deposited from coarse YSZ powder have almost the same content of vertical and horizontal pores.

3.3. Characteristic Parameter of Pore Orientation

In this study, the ceramic coating prepared by agglomerated sintered YSZ powder has a complex pore structure composed of voids and micro-cracks with various shape and orientation. The brick-wall model for APS coatings proposed by McPherson [30] could not be applied to describe the pore structure of the coatings of this investigation. In addition, studies [33,41,42] have shown that the thermal conductivity and elastic modulus of the coating varies with the shape, size, orientation, and location of pores, even though the porosity of coatings is same. Therefore, it is necessary to find a reasonable method to extract the pore orientation features and then to parameterize them.

The above results have shown that the coatings from different size of particles have the different porosity of vertical and horizontal pores. To describe the pore features, the coating with similar porosity was used as the study object. From Figure 9 we found that after 20 cycles of thermal shock, the coatings of different sized particles have a similar total porosity, whose pore structure is shown in Figure 8c,g. It is obvious that the orientation and distribution of the pores are different. The pores in the coating are classified based on the pore analysis method proposed in Section 2.3, whose distribution with the orientation angle is shown in Figure 10a. The pores in the coatings prepared by the fine YSZ particles are dominated by 0° to 30° pores, and the pore content tends to decrease with the increment of orientation angle. The change tendency of the porosity prepared by the coarse YSZ particles is not obvious with the angle, only that of the pore content of 50°–80°, showing a slight increase. The relative change tendency was characterize by the change of the cumulative pore content with orientation angle, which shows a linear relationship in logarithmic coordinate. For the coatings after 20 cycles, the cumulative pore content is shown in Figure 10b. The slope K of the fitted line reflects the orientation angle distribution of pores, which can be used as the quantitative parameter for the pore orientation feature of the coating.

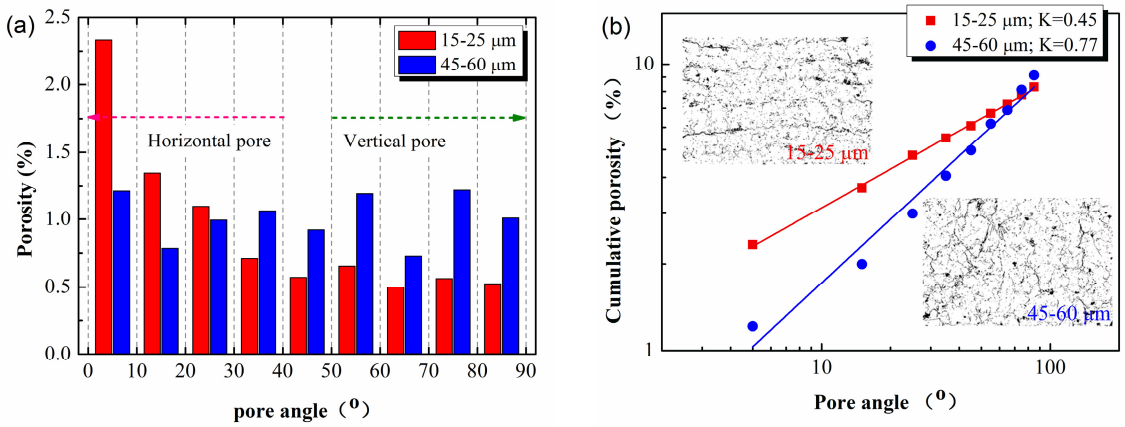

Figure 10. Orientation characteristics of the pore of the two coatings after 20 cycles: (**a**) The distribution of the pore content of the coating with its orientation angle; and (**b**) the change of cumulative pore content in logarithmic coordinates with its orientation angle.

Figure 11 shows the changes of the pore structure parameters K of the two coatings after different cycles of thermal shock. The parameters K of the as-sprayed coatings deposited from different YSZ powder are similar. After heat pre-treatment and cyclic thermal shock testing, the parameter K of the coating prepared by the coarse powder increases, while that by fine powder is reduced. The difference in the parameter K reflects that the pore features in the two kinds of coatings have experienced different evolution. It can be found that for the as-sprayed coatings, the pore feature is determined by the

spraying process. Though the initial particle size and the total coating porosity are different, the relative changing tendency of the horizontal to the vertical pores is similar for the as-sprayed coatings. After the heat pre-treatment and thermal shock, the pores in the coating consist of the initial porosity and the micro-cracks generated by the coupling effect of sintering and thermal stress. The increment of K shows the relative rise in the number of vertical pores comparing with the horizontal ones. In contrast, the decrease of *K* means the rise in the number of horizontal pores. Therefore, from Figure 11, it can be determined that the number of vertical pores is increased more obviously compared with the horizontal ones for the coatings prepared by coarse powder after thermal cycles. For the fine coat, more horizontal pores are formed.

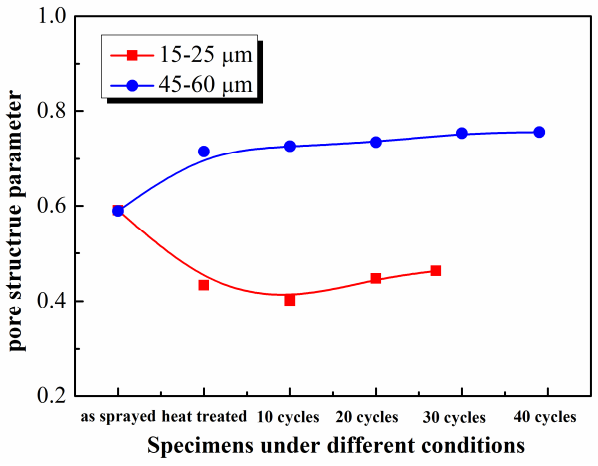

Figure 11. Variation of pore structure parameters *K* of coatings during thermal shocks.

3.4. Influence of Pore Orientation on Thermal Shock Resistance of TBCs

The thermal shock life of the coating prepared by coarse YSZ particles is higher than that made from fine ones. The failure modes of the two coatings are similar. The cracking of both coatings is initiated from the BC/substrate interface during thermal shocks. The cracking propagation in TC layer during thermal shocks has been studied in our previous work [15]. Now the effect of the orientation of pores will be investigated on the stress distribution by FEM simulation. The results are shown in Figure 12. The maximum stress perpendicular to the substrate (S22) locates near the interface of BC/substrate at the edge. The simulation results are in agreement with the experimental results. The location of the peeling-off is consistent with that of the maximum stress.

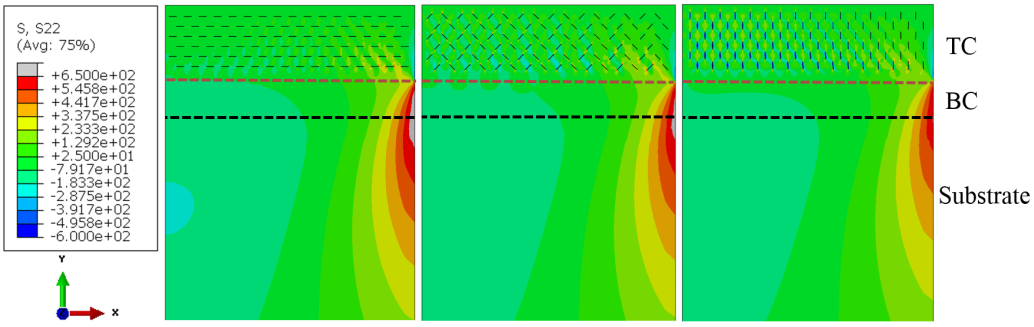

Figure 12. Thermal stress distribution in TBC system with different pore structure during quenching.

The influence of the orientation of pores in the TC layer on the thermal stress is shown in Figure 13. As the pore orientation changes from horizontal to vertical, the maximum stress at the BC/substrate interface shows a decreasing trend during both the insulation stage and the quenching

process. In addition, though the pore angles are different, the stress distributions in the coating are similar. However, the area of the high stress region near the BC/substrate interface of the coating is gradually reduced. The presence of vertical pores can improve the strain tolerance of the coating and reduce the stress caused by the thermal expansion mismatch between the metallic and the ceramic layer. Fracture toughness is an important factor affecting the thermal shock performance of TBCs. In this study, the fracture toughness of the ceramic coatings prepared by the two kinds of powders may be different, which can be inferred from the difference in micro-cracks of the two kinds of coatings after thermal shocks. However, it should be noted that the fracture of all the samples in this experiment occurs in the bond coat near the BC/substrate interface, and the BC layers of the two coatings are the same and undergo the same heat treatment. Therefore, the difference of the thermal shock life between the two coatings is mainly due to the different stress state of the coating system which is related to the pore structures. The toughness of the ceramic layer may affect the pore structure of the coatings, thereby affecting the stress in the TBC system. Therefore, it can be inferred that the coatings prepared by coarse YSZ powders suffer less thermal stress due to the presence of vertical pores, thus, having better thermal shock resistance.

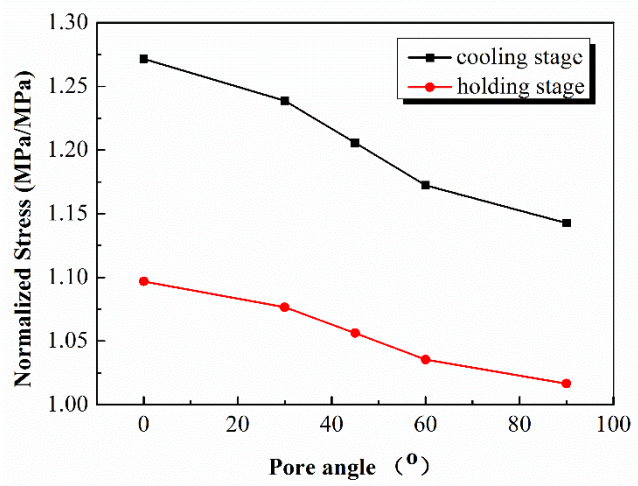

Figure 13. Influence of pore orientation on thermal stress (S22) of TBCs.

4. Conclusions

In this study, the effect of YSZ particle size on the pore structure and thermal shock resistance of the coatings was investigated. Coatings prepared by coarse YSZ powder tend to form almost the same number of horizontal and vertical pores, while coatings prepared by fine powder tend to form horizontal ones parallel to the substrate. The change of the cumulative pore content with orientation angle shows a linear relationship in logarithmic coordinate. The slope K is used as a quantitative parameter describing the pore orientation feature of the coating. The coatings deposited using coarse YSZ particles show the higher thermal shock life due to the presence of relatively less horizontal pores. As the pore orientation changes from horizontal to vertical, the maximum stress shows a decreasing trend both during the insulation stage and the quenching process.

Acknowledgments: The authors gratefully appreciate the support of National Natural Science Foundation of China (No. 51775189), Science and Technology Commission of Shanghai Municipality Project (16DZ2260604), Aviation funding (2015ZES7001) and Shanghai Pujiang Program (15PJD009).

Author Contributions: Jibo Huang and Weize Wang conceived designed the experiments; Jibo Huang, Xiang Lu, Doudou Hu, Zhengqu Feng, Tianxu Guo performed the experiments; and Jibo Huang and Weize Wang analyzed the data and wrote the paper.

Conflicts of Interest: The authors declare no conflict of interest.

References

1. Padture, N.P.; Gell, M.; Jordan, E.H. Thermal barrier coatings for gas-turbine engine applications. *Science* **2002**, *296*, 280–284. [CrossRef] [PubMed]
2. Schulz, U.; Leyens, C.; Fritscher, K.; Peters, M.; Saruhan-Brings, B.; Lavigne, O.; Donvaux, J.-M.; Poulain, M.; Mèvrel, R.; Michaël, C. Some recent trends in research and technology of advanced thermal barrier coatings. *Aerosp. Sci. Technol.* **2003**, *7*, 73–80. [CrossRef]
3. Gan, Z.; Ng, H.N. Experiments and inelastic finite element analyses of plasma sprayed graded coatings under cyclic thermal shock. *Mater. Sci. Eng. A* **2004**, *385*, 314–324. [CrossRef]
4. Kim, D.J.; Shin, I.H.; Koo, J.M.; Seok, C.S.; Lee, T.W. Failure mechanisms of coin-type plasma-sprayed thermal barrier coatings with thermal fatigue. *Surf. Coat. Technol.* **2010**, *205*, S451–S458. [CrossRef]
5. Fauchais, P.; Vardelle, M.; Goutier, S. Latest researches advances of plasma spraying: From splat to coating formation. *J. Therm. Spray Technol.* **2016**, *25*, 1534–1553. [CrossRef]
6. Mutter, M.; Mauer, G.; Mücke, R.; Guillon, O.; Vaßen, R. Correlation of splat morphologies with porosity and residual stress in plasma-sprayed YSZ coatings. *Surf. Coat. Technol.* **2017**, *318*, 157–169. [CrossRef]
7. Ann, J.; Berndt, C.C. Quantification and taxonomy of pores in thermal spray coatings by image;analysis and stereology approach. *Metall. Mater. Trans. A* **2013**, *44*, 4844–4858.
8. Kulkarni, A.; Wang, Z.; Nakamura, T.; Sampath, S.; Goland, A.; Herman, H.; Allen, J.; Ilavsky, J.; Long, G.; Frahm, J. Comprehensive microstructural characterization and predictive property modeling of plasma-sprayed zirconia coatings. *Acta Mater.* **2003**, *51*, 2457–2475. [CrossRef]
9. Sobhanverdi, R.; Akbari, A. Porosity and microstructural features of plasma sprayed yttria stabilized zirconia thermal barrier coatings. *Ceram. Int.* **2015**, *41*, 14517–14528. [CrossRef]
10. Liu, T.; Luo, X.-T.; Chen, X.; Yang, G.-J.; Li, C.-X.; Li, C.-J. Morphology and size evolution of interlamellar two-dimensional pores in plasma-sprayed $La_2Zr_2O_7$ coatings during thermal exposure at 1300 °C. *J. Therm. Spray Technol.* **2015**, *24*, 739–748. [CrossRef]
11. Giolli, C.; Scrivani, A.; Rizzi, G.; Borgioli, F.; Bolelli, G.; Lusvarghi, L. Failure mechanism for thermal fatigue of thermal barrier coating systems. *J. Therm. Spray Technol.* **2009**, *18*, 223–230. [CrossRef]
12. Paul, S. Stiffness of plasma sprayed thermal barrier coatings. *Coatings* **2017**, *7*, 68. [CrossRef]
13. Xiaofeng, Z.; Kesong, Z.; Huantao, C.; Tao, H.; Jinbing, S.; Min, L. Properties of thermal barrier coatings made of different shapes of ZrO_2–7 wt % Y_2O_3 powders. *Rare Met. Mater. Eng.* **2015**, *44*, 1301–1306. [CrossRef]
14. Yu, Z.; Huang, J.; Wang, W.; Yu, J.; Wu, L. Deposition and properties of a multilayered thermal barrier coating. *Surf. Coat. Technol.* **2016**, *288*, 126–134. [CrossRef]
15. Huang, J.; Wang, W.; Yu, J.; Wu, L.; Feng, Z. Effect of particle size on the micro-cracking of plasma-sprayed YSZ coatings during thermal cycle testing. *J. Therm. Spray Technol.* **2017**, *26*, 755–763. [CrossRef]
16. Beele, W.; Marijnissen, G.; Van Lieshout, A. The evolution of thermal barrier coatings—Status and upcoming solutions for today's key issues. *Surf. Coat. Technol.* **1999**, *120*, 61–67. [CrossRef]
17. Song, D.; Paik, U.; Guo, X.; Zhang, J.; Woo, T.-K.; Lu, Z.; Jung, S.-H.; Lee, J.-H.; Jung, Y.-G. Microstructure design for blended feedstock and its thermal durability in lanthanum zirconate based thermal barrier coatings. *Surf. Coat. Technol.* **2016**, *308*, 40–49. [CrossRef]
18. Bakan, E.; Mack, D.E.; Mauer, G.; Mücke, R.; Vaßen, R. Porosity–property relationships of plasma-sprayed $Gd_2Zr_2O_7$/YSZ thermal barrier coatings. *J. Am. Ceram. Soc.* **2015**, *98*, 2647–2654. [CrossRef]
19. Wang, L.; Wang, Y.; Sun, X.; He, J.; Pan, Z.; Zhou, Y.; Wu, P. Influence of pores on the thermal insulation behavior of thermal barrier coatings prepared by atmospheric plasma spray. *Mater. Des.* **2011**, *32*, 36–47. [CrossRef]
20. Gupta, M.; Dwivedi, G.; Nylén, P.; Vackel, A.; Sampath, S. An experimental study of microstructure-property relationships in thermal barrier coatings. *J. Therm. Spray Technol.* **2013**, *22*, 659–670. [CrossRef]
21. Mauer, G.; Du, L.; Vaßen, R. Atmospheric plasma spraying of single phase lanthanum zirconate thermal barrier coatings with optimized porosity. *Coatings* **2016**, *6*, 49. [CrossRef]
22. Bengtsson, P.; Johannesson, T. Characterization of microstructural defects in plasma-sprayed thermal barrier coatings. *J. Therm. Spray Technol.* **1995**, *4*, 245–251. [CrossRef]
23. Tan, Y.; Srinivasan, V.; Nakamura, T.; Sampath, S.; Bertrand, P.; Bertrand, G. Optimizing compliance and thermal conductivity of plasma sprayed thermal barrier coatings via controlled powders and processing strategies. *J. Therm. Spray Technol.* **2012**, *21*, 950–962. [CrossRef]

24. Karger, M.; Vaßen, R.; Stöver, D. Atmospheric plasma sprayed thermal barrier coatings with high segmentation crack densities: Spraying process, microstructure and thermal cycling behavior. *Surf. Coat. Technol.* **2011**, *206*, 16–23. [CrossRef]
25. Guo, H.; Murakami, H.; Kuroda, S. Effect of hollow spherical powder size distribution on porosity and segmentation cracks in thermal barrier coatings. *J. Am. Ceram. Soc.* **2006**, *89*, 3797–3804. [CrossRef]
26. Lu, Z.; Myoung, S.-W.; Kim, H.-S.; Kim, M.-S.; Lee, J.-H.; Jung, Y.-G.; Jang, J.-C.; Paik, U. Microstructure evolution and interface stability of thermal barrier coatings with vertical type cracks in cyclic thermal exposure. *J. Therm. Spray Technol.* **2013**, *22*, 671–679. [CrossRef]
27. Guo, H.; Murakami, H.; Kuroda, S. Effects of heat treatment on microstructures and physical properties of segmented thermal barrier coatings. *Mater. Trans.* **2005**, *46*, 1775–1778. [CrossRef]
28. Pin, L.; Ansart, F.; Bonino, J.-P.; Le Maoult, Y.; Vidal, V.; Lours, P. Reinforced sol–gel thermal barrier coatings and their cyclic oxidation life. *J. Eur. Ceram. Soc.* **2013**, *33*, 269–276. [CrossRef]
29. Pin, L.; Vidal, V.; Blas, F.; Ansart, F.; Duluard, S.; Bonino, J.-P.; Le Maoult, Y.; Lours, P. Optimized sol–gel thermal barrier coatings for long-term cyclic oxidation life. *J. Eur. Ceram. Soc.* **2014**, *34*, 961–974. [CrossRef]
30. McPherson, R. A review of microstructure and properties of plasma sprayed ceramic coatings. *Surf. Coat. Technol.* **1989**, *39*, 173–181. [CrossRef]
31. Chang-Jiu, L.; Wang, W.-Z. Quantitative characterization of lamellar microstructure of plasma-sprayed ceramic coatings through visualization of void distribution. *Mater. Sci. Eng. A* **2004**, *386*, 10–19.
32. Li, C.J.; Ohmori, A. Relationships between the microstructure and properties of thermally sprayed deposits. *J. Therm. Spray Technol.* **2002**, *11*, 365–374. [CrossRef]
33. Sevostianov, I.; Kachanov, M.; Ruud, J.; Lorraine, P.; Dubois, M. Quantitative characterization of microstructures of plasma-sprayed coatings and their conductive and elastic properties. *Mate. Sci. Eng. A* **2004**, *386*, 164–174. [CrossRef]
34. Kulkarni, A.; Vaidya, A.; Goland, A.; Sampath, S.; Herman, H. Processing effects on porosity-property correlations in plasma sprayed yttria-stabilized zirconia coatings. *Mater. Sci. Eng. A* **2003**, *359*, 100–111. [CrossRef]
35. Dwivedi, G.; Viswanathan, V.; Sampath, S.; Shyam, A.; Lara-Curzio, E. Fracture toughness of plasma-sprayed thermal barrier ceramics: Influence of processing, microstructure, and thermal aging. *J. Am. Ceram. Soc.* **2014**, *97*, 2736–2744. [CrossRef]
36. Cheng, B.; Yang, N.; Zhang, Q.; Zhang, Y.-M.; Chen, L.; Yang, G.-J.; Li, C.-X.; Li, C.-J. Sintering induced the failure behavior of dense vertically crack and lamellar structured tbcs with equivalent thermal insulation performance. *Ceram. Int.* **2017**. In Press. [CrossRef]
37. Deshpande, S.; Kulkarni, A.; Sampath, S.; Herman, H. Application of image analysis for characterization of porosity in thermal spray coatings and correlation with small angle neutron scattering. *Surf. Coat. Technol.* **2004**, *187*, 6–16. [CrossRef]
38. Li, J.F.; Li, L.; Stott, F.H. Fractal characteristics of apparent pores present on polished cross sections of alumina coatings prepared by laser-assisted flame hybrid spraying. *Thin Solid Films* **2004**, *453–454*, 229–233. [CrossRef]
39. Shen, W.; Wang, F.C.; Fan, Q.B.; Hua, D.; Ma, Z. Proposal of new expressions for effects of splat interfaces and defects on effective properties of thermal barrier coatings. *Surf. Coat. Technol.* **2010**, *204*, 3376–3381.
40. Zhou, C.; Wang, N.; Xu, H. Comparison of thermal cycling behavior of plasma-sprayed nanostructured and traditional thermal barrier coatings. *Mater. Sci. Eng. A* **2007**, *452–453*, 569–574. [CrossRef]
41. Sevostianov, I.; Kachanov, M. Anisotropic thermal conductivities of plasma-sprayed thermal barrier coatings in relation to the microstructure. *J. Therm. Spray Technol.* **2000**, *9*, 478–482. [CrossRef]
42. Sevostianov, I.; Kachanov, M. Plasma-sprayed ceramic coatings: Anisotropic elastic and conductive properties in relation to the microstructure; cross-property correlations. *Mater. Sci. Eng. A* **2001**, *297*, 235–243. [CrossRef]

© 2017 by the authors. Licensee MDPI, Basel, Switzerland. This article is an open access article distributed under the terms and conditions of the Creative Commons Attribution (CC BY) license (http://creativecommons.org/licenses/by/4.0/).